Physica D 36 (1989) 111–136
North-Holland, Amsterdam

A SIMPLE MODEL FOR CHAOTIC SCATTERING

II. QUANTUM MECHANICAL THEORY

R. BLÜMEL and U. SMILANSKY
Max-Planck-Institut für Quantenoptik, D-8046 Garching, Fed. Rep. Germany and The Weizmann Institute of Science, 76100 Rehovot, Israel

Received 22 September 1988
Accepted 15 January 1989
Communicated by H. Flaschka

In this paper we present the quantum analysis of a scattering problem which displays chaotic (irregular) features when analyzed classically. We treat the problem both semi-classically and exactly and show that the "finger print" of the classical chaos on the quantum description is the appearance of universal fluctuations in the cross section. Their statistics is analogous to the one expected from a random matrix description.

1. Introduction

In the first paper in this series [1] (to be referred to as CT), we have studied the classical theory of a model which displays a transition from regular to chaotic scattering. The model is simple enough to be analyzed analytically, and was used to illustrate the mechanism which is responsible for the chaotic behaviour, and the parameters which characterize it [2]. In the present work we present the semi-classical and quantum mechanical description of the same model, and use them to add more evidence in favour of our proposition [3] that chaotic classical scattering leads to fluctuations in the quantum mechanical scattering matrix, and that the statistical properties of these fluctuations are given by the theory of random (unitary symmetric) matrix ensembles [4–13].

The connection between random matrix theory and the quantal description of classically chaotic dynamics was first established in the study of bounded systems [14, 15]: The spectral fluctuations of Hamiltonians which induce chaotic dynamics in the classical limit behave according to the statistics prescribed by random matrix theory. The agreement between the random matrix theory and the distribution of spectral fluctuations is universal, albeit limited to those ranges of correlations to which a semi-classical treatment (in terms of classical trajectories) is relevant (see ref. [15] for a detailed discussion of this point). Our results indicate that the connection between the quantum mechanics of classically chaotic systems and random matrix theory can be extended also to scattering problems.

The application of random matrix theory to scattering was first introduced in the description of Ericson fluctuations [4–7] observed in nuclear reaction cross sections. Ericson and Mayer-Kuckuk [5] proposed a simple model to illustrate the mechanism which induces the fluctuations. They considered a wave scattered from a cavity with an opening. It was assumed that the wavelength is short in comparison with the

diameter of the opening, which is smaller than a typical linear dimension of the cavity. In this limit, the scattering amplitude is given in terms of overlapping resonances, which is the condition for the resulting fluctuations in the cross section. At the time (~ 1960), the study of chaos in classical mechanics was just emerging, and the fact that the model is nothing but a leaky stadium was not appreciated. In the present series of papers we are trying to establish the link between the quantal fluctuations and the underlying classical chaos by casting Ericson's intuitive picture into the modern and better understood concepts of classical and quantum chaology.

There were a few attempts to study the quantum analogue of chaotic scattering by means of other tools rather than random matrix theory. Gutzwiller [16] studied elastic scattering on a two-dimensional surface of constant negative curvature. He was able to show that the phase shift for scattering from a torus is given essentially by the phase of the Riemann ζ function on the line $z = 1 + 2iw$, where w is the wave number. As a function of w, the phase shift displays a very complicated behaviour, which Gutzwiller calls chaotic because of the following property of the ζ function in the "critical" strip $\frac{1}{2} \leq \mathrm{Re}\, z \leq 1$: Consider a disc C in the "critical" strip and a function $f(z)$ analytic and non-vanishing in C. Then for any real Δ one can find infinitely many integers l such that $\zeta(z + il\Delta)$ approximates $f(z)$ to any desired accuracy in C. Since this is true for all possible choices of f, one can say that the ζ function has no typical behaviour. In other words, the ζ function in the critical strip embodies all possible functions, and may be thought of as itself representing the ensemble of all analytic (non-vanishing) functions in C.

In the study of atomic and molecular reactions, there were various attempts to predict features of the quantum cross sections by relating them to the underlying classical chaos. A summary of this work and an exhaustive list of references is given in a recent review paper by Brumer and Shapiro [17]. In spite of the deep physical understanding derived from these studies, and the abundant numerical evidence which was accumulated, the link to the theory of random ensembles (of matrices or functions) was not made.

We shall start the paper by introducing the physical model in a way which will be convenient for the subsequent discussion (section 2). We shall then present the semi-classical theory for the scattering amplitude and compare the results for situations where the classical scattering is either regular or chaotic (section 3). The complete quantum theory will follow (section 4), and a closed analytical expression for the S-matrix will be given. The statistics of the S-matrix will be studied in section 5 and will be compared to the predictions of random matrix theory.

2. The model

We consider a particle of mass m confined to move in a plane. It scatters from an infinite array of non-overlapping scatterers (shaded discs in fig. 1), placed at constant intervals D along the y axis. Each scatterer is represented by a spherical potential $v(|r|)$ which is confined to a circle of diameter $d < D$:

$$v(r) = 0 \quad \text{for } r > d/2. \tag{2.1}$$

The effect of any single scatterer is completely specified once the phase shifts $\sigma_l(E)$ are given. The phase shifts are related to the elastic reaction matrix $T_l(E)$ and the elastic scattering matrix $S_l(E)$ through the relation

$$T_l = \tfrac{1}{2}(S_l - 1) = \mathrm{i}e^{\mathrm{i}\sigma_l} \sin(\sigma_l) = -\frac{\mathrm{i}\pi m}{\hbar^2} \int_0^\infty r' J_l(kr') v(r') \psi_l^{(+)}(r')\, \mathrm{d}r', \tag{2.2}$$

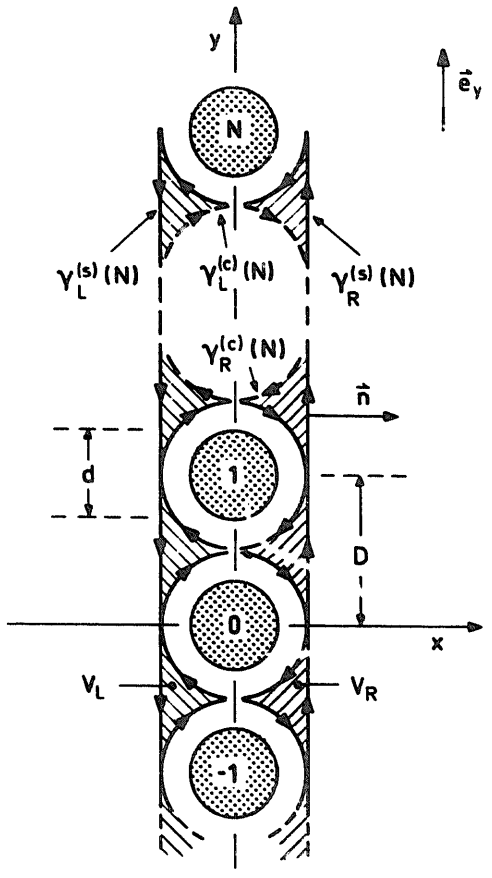

Fig. 1. Sketch of the periodic array of scattering discs (shaded areas). The path $\gamma_R(N) = \gamma_R^{(s)}(N) + \gamma_R^{(c)}(N)(\gamma_L(N) = \gamma_L^{(s)}(N) + \gamma_L^{(c)}(N))$ encloses the volume $V_R(N)$ $(V_L(N))$ (hatched areas).

where $\psi_l^{(+)}(r)$ is the solution of the Schrödinger equation for a single scatterer with outgoing wave boundary condition:

$$\psi_l^{(+)}(r) = J_l(kr) + T_l H_l^{(+)}(kr), \quad r \geq d/2. \tag{2.3}$$

We shall make extensive use of the 2-D Green's function [18] which satisfies

$$[\Delta + k^2] G_k^{(+)}(r; r') = -4\pi\delta(r - r') \tag{2.4}$$

subject to outgoing wave boundary conditions. $G_k^{(+)}(r; r')$ is explicitly given by

$$G_k^{(+)}(r, r') = i\pi \sum_{m=-\infty}^{\infty} e^{im(\tilde{\varphi}_r - \tilde{\varphi}_{r'})} J_m(kr_<) H_m^{(+)}(kr_>). \tag{2.5}$$

The combined effect of the entire array of potentials is given by the union of the individual scattering potentials:

$$V(r) = \sum_{n=-\infty}^{\infty} v(|r - r_n|), \tag{2.6}$$

where

$$r_n = nDe_y, \quad n = 0, \pm 1, \pm 2, \ldots . \tag{2.7}$$

Because of the discrete translational symmetry in the y direction, the wavefunctions must satisfy the Bloch condition:

$$\psi^{(\alpha)}(x, y) = e^{i\alpha y} \varphi^{(\alpha)}(x, y), \tag{2.8}$$

where $\varphi^{(\alpha)}(x, y)$ is D-periodic in y. Hence,

$$\psi^{(\alpha)}(x, y + nD) = e^{in\alpha D} \psi^{(\alpha)}(x, y). \tag{2.9}$$

Reflection and transmission is only possible into a finite number of discrete directions with wave vectors:

$$k_n^{(\pm)} = \begin{pmatrix} \pm p_n \\ q_n \end{pmatrix}, \quad p_n^2 + q_n^2 = k^2.$$

In other words, the discrete translational symmetry implies the quantization of the y component of the momentum: the only values that q can obtain are those which differ from the incoming value q_0 by integer multiples of $2\pi/D$. As a matter of fact α defined above equals q_0. Not all values of $q_n = q_0 + (2\pi/D)n$ are allowed, since by conservation of energy $q_n^2 \leq k^2$. This finite set of allowed directions for transmission and reflection by the array of scatterers is the Bragg manifold. Its dimension will be denoted by N_B.

To obtain the transmission and reflection coefficients within a given Bragg manifold we make a partial Fourier expansion of the wavefunction

$$\psi^{(\alpha)}(x, y) = e^{i\alpha y} \sum_{m=-\infty}^{\infty} \varphi_m^{(\alpha)}(x) e^{im(2\pi/D)y}. \tag{2.10}$$

This expansion is substituted into the stationary Schrödinger equation which yields a set of coupled equations for the expansion coefficients $\varphi_m^{(\alpha)}$:

$$-\varphi_n^{(\alpha)\prime\prime}(x) + \frac{2m}{\hbar^2} \sum_m \tilde{v}_{n-m}(x) \varphi_m^{(\alpha)}(x) = p_n^2 \varphi_n^{(\alpha)}(x), \tag{2.11}$$

where

$$\tilde{v}_{n-m}(x) = \frac{1}{D} \int_{-D/2}^{D/2} e^{-i(n-m)(2\pi/D)y} v(x, y)\, dy \tag{2.12}$$

and

$$p_n = \begin{cases} \sqrt{k^2 - q_n^2} & \text{for "open" channels,} \\ i\sqrt{q_n^2 - k^2} & \text{for "closed" channels,} \end{cases} \tag{2.13}$$

(2.11) has to be solved with the boundary conditions:

$$\psi^{(\alpha)}(x,y)=\frac{1}{\sqrt{p_0}}e^{ip_0x+iq_0y}+\sum_{n=-\infty}^{\infty}\frac{1}{\sqrt{p_n}}r_{n,0}e^{-ip_nx+iq_ny}\quad\text{for } x<-d/2, \tag{2.14}$$

$$\psi^{(\alpha)}(x,y)=\sum_{n=-\infty}^{\infty}\frac{1}{\sqrt{p_n}}t_{n,0}e^{ip_nx+iq_ny}\quad\text{for } x>d/2, \tag{2.15}$$

where $r_{n,0}$ and $t_{n,0}$ are the reflection and transmission coefficients. We have denoted the incoming direction by the index "0", but this choice is completely arbitrary. Any allowed direction within the Bragg manifold can serve as an incoming direction, and therefore eqs. (2.14, 15) define the transmission and reflection matrices $t_{n,m}$ and $r_{n,m}$. The system is symmetric under reflections about the x axis. Hence, the S-matrix can be written as

$$S=\begin{pmatrix} t & r \\ r & t \end{pmatrix}, \tag{2.16}$$

which, by a suitable orthogonal transformation, can be reduced to the final form

$$S=\begin{pmatrix} S^{(+)} & 0 \\ 0 & S^{(-)} \end{pmatrix}=\begin{pmatrix} t+r & 0 \\ 0 & t-r \end{pmatrix}. \tag{2.17}$$

The dimension of the matrices $S^{(+)}$ and $S^{(-)}$ will be denoted by $N_B^{(+)}$ and $N_B^{(-)}$, respectively.

The dimension of the Bragg manifold depends on the energy and on the incident angle. The dimension changes whenever one of the Bragg directions coincides with the y axis. In this case $p_n^2=(k+q_n)\cdot(k-q_n)=0$ and the dimension of the manifold changes by two (or four, for $\alpha=0 \bmod 2\pi/D$). This corresponds to a threshold behaviour of the S-matrix and it requires some special attention.

The formalism which we shall present below is valid for any choice of the single scatterer potential $v(r)$ or the corresponding phase shifts $\sigma_l(E)$. We have shown in CT that the classical treatment takes a very simple form when the classical deflection function is assumed to be linear in the impact parameter. The corresponding semi-classical phase shift is quadratic in l, with a coefficient which depends only on the energy. The actual energy dependence did not concern us in CT. As will be shown below, the connection between the classical and quantum theories is best established in terms of the energy dependence of the cross sections. Hence we have to know what is the energy dependence of the phase shift which is consistent with the prescribed dependence on l. We make use of an approximate relation between the phase shifts and the scattering potential to obtain (see ref. [19], formula 123.2):

$$\sigma_l(E)=2v_0l^2/Ekd, \tag{2.18}$$

where v_0 denotes the depth of the effective scattering potential. This form holds for $l<l_{\max}=kd/2$. For $l>l_{\max}$ the phase shift is set to zero.

3. Semi-classical theory

The analysis presented in CT has shown that in the present system one encounters a transition from regular to chaotic scattering. For the particular choice of phase shifts (2.18), regular dynamics is guaranteed for

$$\Theta_{\max} \leq \pi. \tag{3.1a}$$

$\Theta_{\max}$ is the maximal deflection angle, which, for the phase shifts (2.18), takes the simple form $\Theta_{\max} = 4v_0/E$. Fully developed chaos starts only when

$$\Theta_{\max} \geq \pi + \arcsin(d/D). \tag{3.1b}$$

The transition region is marked by a succession of homoclinic bifurcations [20]. Partial chaos sets in at approximately

$$\Theta_{\max} \approx \pi + \arcsin(d/2D). \tag{3.1c}$$

In the regular regime, the invariant set of the mapping reduces to a single point in phase-space, and the deflection function is a piecewise linear function. The classical deflection function was discussed in section 3.4 in CT. In the chaotic regime, the invariant set is a Cantor set, and the deflection function fluctuates on all scales. In the present section we shall derive a semi-classical expression for the S-matrix in the classically regular regime, and discuss its analytical properties in the complex E plane. In the classically irregular regime, we shall use semi-classical techniques to derive expressions for correlation functions which involve elements of the S-matrix. The correlation functions resemble those expected from random matrix theory, and allow us to make specific predictions on the statistics of the fluctuations.

We shall use the semi-classical reaction theory [21] to write the S-matrix in the form

$$S_{n,m}(E) = \sum_s \left[P^{(s)}_{n\to m}\right]^{1/2} \exp\left(\frac{\mathrm{i}}{\hbar}\Phi^{(s)} - \mathrm{i}\frac{\pi}{2}\nu_s\right), \tag{3.2}$$

where ν_s is the Maslov index [22]. The sum extends over all the classical trajectories which correspond to scattering from the nth to the mth Bragg directions. The corresponding classical probability is

$$P^{(s)}_{n\to m} = \frac{k}{\hbar}\left(p_n p_m \frac{\partial x_f(p_i)}{\partial p_i}\right)^{-1}. \tag{3.3}$$

This expression follows from the relations

$$q = k\cos(x) \tag{3.4}$$

and

$$(y/D) \bmod 1 = p/\sin(x), \tag{3.5}$$

which relates the parameters of the classical mapping (x, p) to the y coordinate and the conjugate momentum $\hbar q$. The function $x_f(p_i)$ is the deflection function which gives the final scattering angle as a

function of the initial impact parameter for a given incidence angle x_i. Here x_i coincides with the nth Bragg direction. The reduced classical action is given by

$$\Phi/\hbar = -\left(\int x\,\mathrm{d}k_x + \int y\,\mathrm{d}k_y\right) = \int k_x\,\mathrm{d}x + \int k_y\,\mathrm{d}y - \left[k_x x + k_y y\right]_i^f. \tag{3.6}$$

For further reference we mention here two important properties of the action Φ. Its derivative with respect to the energy, $\partial\Phi/\partial E$, defines the delay time T which measures the extra time spent by the trajectory in the interaction region. Similarly, $(1/\hbar)(\partial\Phi/\partial q)$ defines the net distance which the particle travelled along the array of scatterers before being scattered away.

Examination of the deflection function (see section 3.4 and fig. 2 in CT) reveales that there may be infinitely many classical trajectories which satisfy the required boundary conditions. In the regime where the classical scattering is regular the deflection function is simple and one can sum the infinite series which is implied by (3.2). In the domain of parameters where the classical scattering is chaotic, the deflection function oscillates on all scales and there is no chance to sum (3.2) analytically. Still, one can use (3.2) to obtain information on correlations between elements of the S-matrix.

i) *Regular domain*

The deflection function is composed of straight sections each of which corresponding to trajectories where the multiplicity of scattering before escape is s and

$$\left[\partial x_f(p_i)/\partial p_i\right]_s = \frac{(\lambda-1)}{(1+\lambda)}(\lambda^s - \lambda^{-s}). \tag{3.7}$$

λ is the largest eigenvalue of the stability matrix and it is related to the Lyapunov exponent by $L = \ln(\lambda)$. (For details see CT section 3.4.)

The trajectories with multiplicity s spend most of their time in the vicinity of the set of bounded trajectories, which, in the present case correspond to trajectories which go up or down the array through the centers of the scattering potentials. We may therefore approximate the action $\phi^{(s)}$ by

$$\phi^{(s)} = s\cdot\phi(E), \quad \phi(E) = 2\sigma_{l=0}(E). \tag{3.8}$$

Substituting (3.7, 8) in (3.2) results in a geometric series which sums up to

$$S_{n,m} \approx \left[\frac{k/\hbar}{p_n p_m}\right]^{1/2}\left[(1+\lambda)/(\lambda-1)\right]^{1/2}\left[1-\exp\left(\frac{\mathrm{i}}{\hbar}\phi - \frac{1}{2}L\right)\right]^{-1}. \tag{3.9}$$

This expression holds whenever the scattering from the nth to the mth Bragg directions is classically allowed, and for the generic cases where the final angle is not too close to the edge of the classically allowed region.

Both the mean action per scattering ϕ and the Lyapunov exponent L depend on the scattering energy E. The poles of the S-matrix (resonances) occur at the complex roots of the equation

$$\phi(E)/\hbar + \frac{\mathrm{i}}{2}L(E) = 2\pi n, \quad n = 0, \pm 1, \pm 2, \ldots. \tag{3.10}$$

The distance between successive resonance energies can be approximately obtained by the requirement that the corresponding differences in the actions is $2\pi\hbar$. This implies that the separation between

successive resonances scales like $\hbar$, and it is determined by a "quantization rule" of the type encountered in the quantization of one-dimensional bounded systems. The width of the resonances is determined by the Lyapunov exponent. In the present case, the Lyapunov exponent and the escape rate γ are equal because the invariant set degenerates to a point in the regular domain and the equality follows immediately from (4.5) in CT. Thus, the width is related, as usual, to the lifetime of the resonance and it scales as $\hbar$. For the phase shifts (2.18), we get $\sigma_{l=0}(E) = 0$. Hence, we do not expect poles in the vicinity of the real energy axis, and the only large variations in the cross sections occur when a threshold condition is encountered (fig. 6).

The analytical treatment of the classical deflection function (section 3.4 in CT) shows that not all final directions are allowed for a given incident angle. This restricts the pairs of Bragg directions between which reflection or transmission can occur, and the corresponding S-matrix elements are exponentially small. Thus, the S-matrix is expected to be sparse.

ii) *Chaotic domain*

The classical deflection function in this domain of parameters displays all the complexity which characterizes chaotic scattering. The number of trajectories which satisfy the prescribed boundary conditions is not denumerable, and a direct application of eq. (3.2) is impossible. In ref. [3] we were able to use semi-classical arguments to calculate correlations between elements of the S-matrix, and propose a link to the random matrix description of scattering. We shall outline the derivation, provide a few details and list the main results pertaining to the S-matrix fluctuations. The degree by which the exact quantal S-matrix obeys the statistics proposed by the semi-classical argument, will be discussed in section 5.

Here, and in the following, we consider the S-matrix in its reduced form (2.17). Thus S stands for either $S^{(+)}$ or $S^{(-)}$ and we omit the sign for brevity. In the same way we shall use the symbol N_B for the dimensionality of either subspaces of the Bragg manifold (see end of section 2).

In the present problem it is safe to assume that all the classical trajectories which contribute to the sum (3.2) are chaotic. (This is not true in general, and in most cases one should treat separately the contributions from regular and chaotic trajectories.)

We consider first the autocorrelation functions

$$F_{nm}(\eta) = N_B \langle S^*_{nm}(E) S_{nm'}(E) \rangle_n, \tag{3.11}$$

where $\eta = m' - m$, and $\langle\ \rangle_n$ denotes averaging over a small domain Δn of n and m, keeping η constant. The size of Δn will be discussed below. The function $F_{nm}(\eta)$ measures the degree by which the S-matrix elements are correlated on average. It is normalized in such a way that $F_{nn}(\eta = 0)$ ranges between the values N_B if the S-matrix is diagonal, and 1 if the S-matrix elements are distributed at random, subject to the unitarity condition. Thus, $F_{nm}(\eta)$ measures the statistical properties of the S-matrix at a given energy.

Substituting (3.2) in (3.11), we get to lowest order in η

$$F_{nm}(\eta) = \left\langle \sum_s P^{(s)}_{n\to m} \exp\left(\frac{2\pi i \eta}{D\hbar} \frac{\partial \Phi^{(s)}}{\partial q_m} \right) \right\rangle_n + \left\langle \sum_{s \neq s'} \left(P^{(s)}_{n\to m} P^{(s')}_{n\to m'} \right)^{1/2} \exp\left(\frac{i}{\hbar} (\Phi^{(s)} - \Phi^{(s')}) - \frac{i\pi}{2} (\alpha_s - \alpha_{s'}) \right) \right\rangle_n . \tag{3.12}$$

The phase factor in the second term involves differences of classical actions from different trajectories. Choosing Δn such that the corresponding variations in the classical momenta $(2\pi/D)\hbar\,\Delta n$ will be large on

the quantum scale, but small on the classical scale, the contribution of the double sum in eq. (3.12) averages out. In the first term we replace $(1/\hbar)(\partial\Phi^{(s)}/\partial q_m)/D$ by $Y^{(s)}$, which measures the net distance travelled along the y direction in units of D. We now use Y to label the trajectories and we get

$$F_{nm}(\eta) \sim \left\langle \sum_s P_{n\to m}^{(s)} \exp\left(\frac{2\pi i\eta}{D\hbar} \frac{\partial\Phi^{(s)}}{\partial q_m} \right) \right\rangle_n$$
$$\sim \int dY \left\langle \tilde{P}_{nm}(Y) \right\rangle_n \exp(2\pi i\eta Y). \tag{3.13}$$

$\tilde{P}_{nm}(Y)$ is the probability that in a scattering from the nth to the mth Bragg direction, the classical trajectory will travel a net distance $Y \cdot D$ along the array. This function was discussed in section 4.2 in CT and was shown to behave as $\exp(-\beta|Y|)$ where β is independent of n or m and its value is given explicitly in CT. Hence

$$F_{nm}(\eta) \sim \frac{F_{nm}(0)}{(1 - 2i\pi\eta/\beta)}. \tag{3.14}$$

η can assume only integer values and in the present case $\beta < 2\pi$. Thus, even the correlations between neighbouring elements of the S-matrix are small. The only constraint on S is that it is unitary and symmetric. These observations lead us to propose that the statistical properties of the S-matrix are determined by the rules which hold for Dyson's orthogonal ensemble of random unitary matrices [8, 23]. If this is indeed the case, it follows that in the limit $N_B \gg 1$:

(a) The nearest neighbour distribution of the eigenvalues of the S-matrix on the unit circle is a Wigner function.

(b) At a given energy, the distribution of $|S_{nm}|^2$ is Poissonian with a mean of $1/N_B$ for off-diagonals and $2/N_B$ for diagonal elements. (Explicit expressions for the distribution law, valid for arbitrary values of N_B, are given in ref. [23].)

Consider now S-matrices calculated at different energies. If there were no correlations in energy, these matrices would represent arbitrary choices of members of the ensemble. Therefore, the distribution of $|S_{nm}(E)|^2$ for a *particular* choice of n and m, when E is varied, should be Poissonian. But, this implies that the $n \to m$ transition probability considered as a function of E has the highest probability to obtain values close to zero, or, in other words, the transition probabilities should fluctuate as a function of energy. Most of the time their value should be less than the average value $(1 + \delta_{nm})/N_B$.

Correlations in energy do exist and to discuss them quantitatively we now turn to the autocorrelation function

$$C_{nm}(\epsilon) = \langle S_{nm}^*(E) S_{nm}(E+\epsilon) \rangle_E, \tag{3.15}$$

where $\langle\ \rangle_E$ denotes averaging over a classically small energy interval ΔE, whose size will be discussed below.

Using the same arguments as were used for the calculation of $F_{nm}(\eta)$ and choosing ΔE large on the quantum scale to allow neglecting the contribution from different trajectories we get

$$C_{nm}(\epsilon) = \int dT \langle \tilde{P}_{nm}(E,T) \rangle_E \exp(i\epsilon T/\hbar). \tag{3.16}$$

$\tilde{P}_{nm}(E,T)$ is the classical probability that an $n \to m$ transition occurs while the delay time is in the interval

$[T, T + \mathrm{d}T]$. The classical theory shows that $\tilde{P}_{nm}(E, T) \sim \exp(-\gamma(E)T)$, and γ is independent of n or m. Explicit expressions for γ and its relation to the parameters which characterize the invariant set of the classical mapping are given in section 4.1 of CT. If ΔE is chosen sufficiently small on the classical scale, so that the variation of γ in the interval can be neglected, we get

$$C_{nm}(\epsilon) = C_{nm}(0)\frac{\gamma}{\gamma - \mathrm{i}\epsilon/\hbar}. \tag{3.17}$$

This equation is valid if the classical and quantum energy scales are sufficiently different and ΔE is chosen in the intermediate range.

We can add three more points to the two results quoted above, concerning the statistical properties of the S-matrix:

(c) The energy dependence of the transmission or reflection probabilities

$$\tau_{nm}(E) = |t_{nm}(E)|^2 \quad \text{and} \quad \rho_{nm}(E) = |r_{nm}(E)|^2 \tag{3.18}$$

will show a typical fluctuation pattern (Ericson fluctuations) [4, 5].

(d) Because of (3.16), autocorrelation functions of the type

$$\langle \tau_{nm}(E)\tau_{nm}(E+\epsilon)\rangle_E \quad \text{and} \quad \langle \rho_{nm}(E)\rho_{nm}(E+\epsilon)\rangle_E \tag{3.19}$$

should show a Lorentzian dependence on ϵ whose width is $\hbar\gamma$.

The qualitative difference between the properties of the S-matrix in the classically regular and classically chaotic regimes can be understood on the following grounds. The density of the resonances is determined semi-classically by the density of periodic orbits. In the regular domain there exists only one such orbit at any given energy, a situation typical for one-dimensional bounded motion. The quantization of this problem leads to a spectrum with spacings which scale like $\hbar$. In the chaotic domain, the number of periodic orbits at a given energy grows exponentially with the period. This is typical for chaotic motion in two dimensions, and the spectral spacings scale as $\hbar^2$. In both regimes, however, the finite mean life of the resonances is due to a classically allowed escape mechanism, and hence, the width of the resonances is always linear in $\hbar$. In the limit $\hbar \to 0$ the S-matrix in the regular regime will continue to be characterized by regularly spaced, non-overlapping resonances. In the chaotic regime, the width will eventually exceed the resonance spacings, and the fluctuations in the S-matrix will be of the Ericson type.

The semi-classical theory presented above relies on the assumption that the actions $\Phi^{(s)}$ for different trajectories with the same boundary conditions are separated by more than $\hbar$. This is fulfilled in the case of regular scattering. For chaotic scattering, we observe that the problem of coalescence of actions $\Phi^{(s)}$ becomes more acute as the delays $T^{(s)}$ are longer. The corresponding probability densities decrease exponentially and hence this regime of T (and Y) values will have little effect on the correlation functions.

The semi-classical theory makes clear and well-defined predictions on the statistical properties of the S-matrix and the observables related to it. In section 5 we shall show that the S-matrices which are calculated quantum mechanically follow the expected statistics to a high degree of accuracy.

4. Quantum theory

To calculate the quantum mechanical S-matrix, we make use of the KKR method [24–26] adapted to the present problem. The calculation proceeds in two steps. First we calculate the scattering wavefunction

in the vicinity of the spherical scattering discs. In a second step, the wavefunction is connected to the asymptotic region by a suitable contour integral, which yields explicit expressions for the reflection and transmission amplitudes.

The scattering wavefunction for the periodic array of scatterers defined in (2.6) satisfies the Lippmann–Schwinger equation:

$$\psi_k^{(\alpha)}(r) = \frac{1}{\sqrt{p_0}} e^{ikr} - \frac{m}{2\pi\hbar^2} \int d^2r' G_k^{(+)}(r; r') V(r') \psi_k^{(\alpha)}(r'), \tag{4.1}$$

where $G_k^{(+)}(r; r')$ is the free space Green's function defined in (2.4, 5). Together with (2.1) and the Bloch condition (2.8, 9) we get

$$\int d^2r' G_k^{(+)}(r; r') V(r') \psi_k^{(\alpha)}(r') = \sum_{n=-\infty}^{\infty} \int_{r' \le d/2} d^2r' G_k^{(+)}(r; r' + nDe_y) v(r') e^{i\alpha n D} \psi_k^{(\alpha)}(r') \tag{4.2}$$

and with the help of the Lattice Green's function

$$g_k^{(+)}(r; r') = \sum_{n=-\infty}^{\infty} G_k^{(+)}(r; r' + nDe_y) e^{in\alpha D} \tag{4.3}$$

(4.1) turns into

$$\psi_k^{(\alpha)}(r) = \frac{1}{\sqrt{p_0}} e^{ikr} - \frac{m}{2\pi\hbar^2} \int_{r' \le d/2} d^2r' g_k^{(+)}(r; r') v(r') \psi_k^{(\alpha)}(r'). \tag{4.4}$$

For $r \le D/2$ the wavefunction is expanded according to

$$\psi_k^{(\alpha)}(r) = \frac{1}{\sqrt{p_0}} \sum_{n=-\infty}^{\infty} a_n(k, \alpha) \psi_n(r) e^{in\Phi_r}, \tag{4.5}$$

where $\psi_n(r)$ are the radial solutions of the single disc scattering problem. In order to calculate the expansion coefficients $a_n(k, \alpha)$, we use (4.4) to calculate the wavefunction $\psi_k^{(\alpha)}(r)$ anywhere inside the ring $d/2 \le r \le D/2$. In this case $D/2 \ge r \ge r'$ and the Lattice Green's function is given by (see appendix A)

$$g_k^{(+)}(r; r') = i\pi \sum_{l,l'=-\infty}^{\infty} \{\delta_{ll'} H_l^{(+)}(kr) + F_{l-l'}(Dk, D\alpha) J_l(kr)\} J_{l'}(kr') e^{i(l\Phi_r - l'\Phi_{r'})}, \tag{4.6}$$

with the "structure function"

$$F_L(x, y) = 2 \sum_{n=1}^{\infty} H_L^{(+)}(xn) \cos\left(yn - L\frac{\pi}{2}\right), \quad |y| \le x, \quad x > 0. \tag{4.7}$$

If now we insert (4.5) and (4.6) into (4.4) and use (2.2) for the radial integrals, we get

$$a_n(k,\alpha)\psi_n(r) = \mathrm{i}^n J_n(kr)\,\mathrm{e}^{-\mathrm{i}n\Phi_k} + \sum_m \{H_m^{(+)}(kr)\delta_{nm} + F_{n-m}(Dk, D\alpha)J_n(kr)\}T_m a_m(k). \tag{4.8}$$

In the ring region we can substitute (2.3) for $\psi_n(r)$ in (4.8). The terms proportional to the Hankel functions drop and comparing the terms proportional to $J_n(kr)$ we get

$$\sum_m \{\delta_{nm} - F_{n-m}(Dk, D\alpha)T_m\}\, a_m(k) = \mathrm{i}^n \mathrm{e}^{-\mathrm{i}n\Phi_k},$$
$$a_{-m}(k,\alpha) = (-1)^m a_m(k,-\alpha). \tag{4.9}$$

Since T_m vanishes quickly for $m > kd/2$, the system (4.9) is essentially of finite dimension. For given phase shifts σ_n this system of inhomogeneous coupled linear equations determines the amplitudes $a_n(k)$. Together with (4.5) and (2.9) this implies that the wavefunction $\psi_k^{(\alpha)}(r)$ is now completely known in discs of radius $D/2$ around the scattering centers r_n.

In order to obtain explicit expressions for the reflection and transmission amplitudes r_n and t_n in (2.14, 15), we connect the spherical (4.5) and cartesian (2.14, 15) representations of the wavefunction in the asymptotic region ($r > d/2$) by suitably chosen contour integrals. Consider the path $\gamma_R(N) = \gamma_R^{(s)}(N) + \gamma_R^{(c)}(N)$ to the right of the y axis in fig. 1. It consists of a straight segment $\gamma_R^{(s)}(N)$ located at $x = D/2$ and ranging from $-ND \le y \le ND$, and the union of quarter- (semi-) circles $\gamma_R^{(c)}(N)$ with radius $D/2$ and $x \ge 0$. The path $\gamma_L(N) = \gamma_L^{(s)}(N) + \gamma_L^{(c)}(N)$ is defined in an analogous way (see fig. 1). γ_R (γ_L) encloses the surface V_R (V_L). For the wavefunction we will use (2.14, 15) for $|x| > D/2$ and (4.5) together with (2.3) for $|x| < D/2$. To project reflection and transmission coefficients from the wavefunction $\psi_k^{(\alpha)}(r)$ we can use the relations (valid for $N \to \infty$ and arbitrary K)

$$\lim_{N\to\infty} \int_{\gamma_R^{(s)}(N)} \mathrm{d}n \left\{\mathrm{e}^{-\mathrm{i}Kr}\nabla\psi_k^{(\alpha)}(r) - \psi_k^{(\alpha)}(r)\nabla\,\mathrm{e}^{-\mathrm{i}Kr}\right\}$$
$$= 2\pi\mathrm{i}\sum_m \frac{1}{\sqrt{p_m}}\delta(q_m - K_y)t_{m,0}(k)(p_m + K_x)\,\mathrm{e}^{\mathrm{i}(p_m - K_x)\cdot D/2} \tag{4.10}$$

and

$$\lim_{N\to\infty} \int_{\gamma_L^{(s)}(N)} \mathrm{d}n \left\{\mathrm{e}^{-\mathrm{i}Kr}\nabla\psi_k^{(\alpha)}(r) - \psi_k^{(\alpha)}(r)\nabla\,\mathrm{e}^{-\mathrm{i}Kr}\right\}$$
$$= 2\pi\mathrm{i}\sum_m \frac{1}{\sqrt{p_m}}\delta(q_m - K_y)r_{m,0}(k)(p_m - K_x)\,\mathrm{e}^{\mathrm{i}(p_m + K_x)\cdot D/2}$$
$$- 2\pi\mathrm{i}\frac{1}{\sqrt{p_0}}\delta(q_0 - K_y)(p_0 + K_x)\,\mathrm{e}^{-\mathrm{i}(p_0 - K_x)\cdot D/2}. \tag{4.11}$$

In the above formuli n is the properly oriented normal on the contours γ_R (γ_L) (see fig. 1). Using Green's theorem on the contour γ_R (γ_L) and the fact that the scattering potential vanishes inside the enclosed

volumes V_R (V_L), we get

$$\int_{\gamma_R(\gamma_L)} d\boldsymbol{n}\left\{e^{-ik_n^{(\pm)}r}\nabla\psi_k^{(\alpha)}(r)-\psi_k^{(\alpha)}(r)\nabla e^{-ik^{(\pm)}r}\right\}$$

$$=\int_{V_R(V_L)} d^2r\left\{e^{-ik_n^{(\pm)}r}\Delta\psi_k^{(\alpha)}(r)-\psi_k^{(\alpha)}(r)\Delta e^{-ik_n^{(\pm)}r}\right\}=0, \tag{4.12}$$

which can be used in connection with (4.10) and (4.11) to relate the reflection and transmission amplitudes to the contour integrals over the (semi-) circles $\gamma_R^{(c)}+\gamma_L^{(c)}$ around the scattering centers:

$$\int_{\gamma_R^{(c)}+\gamma_L^{(c)}} d\boldsymbol{n}\left\{e^{-ik_n^{(\pm)}r}\nabla\psi_k^{(\alpha)}(r)-\psi_k^{(\alpha)}(r)\nabla e^{-ik_n^{(+)}r}\right\}=-\frac{8iN}{\sqrt{p_0}}\sum_m(-i)^m T_m a_m(k)e^{im\Phi_{k_n}(\pm)} \tag{4.13}$$

For large N we have

$$\int_{\gamma_R^{(s)}+\gamma_L^{(s)}} d\boldsymbol{n}\left\{e^{-ik_n^{(+)}r}\nabla\psi_k^{(\alpha)}(r)-\psi_k^{(\alpha)}(r)\nabla e^{-ik_n^{(+)}r}\right\}=4iND\left(\sqrt{p_n}t_n(k)-\sqrt{p_0}\delta_{n0}\right) \tag{4.14}$$

and

$$\int_{\gamma_R^{(s)}+\gamma_L^{(s)}} d\boldsymbol{n}\left\{e^{-ik_n^{(-)}r}\nabla\psi_k^{(\alpha)}(r)-\psi_k^{(\alpha)}(r)\nabla e^{-ik_n^{(-)}r}\right\}=4iND\sqrt{p_n}r_n(k). \tag{4.15}$$

From (4.12) with (4.13)–(4.15) we get

$$\begin{aligned} t_{nm}&=\delta_{nm}+\frac{2}{D\sqrt{p_n p_m}}\sum_l T_l a_l(k_m)e^{il(\Phi_n-\pi/2)},\\ r_{nm}&=\frac{2}{D\sqrt{p_n p_m}}\sum_l T_l a_l(k_m)e^{-il(\Phi_n-\pi/2)}, \end{aligned} \tag{4.16}$$

where instead of the special incoming direction "0" we chose the arbitrary direction "m", and $\Phi_n=\arcsin(q_n/k)$. The reflection and transmission matrices (4.16) are the building blocks of the S-matrix which is constructed according to (2.16, 17).

For the actual calculation of the S-matrix we need the amplitudes a_l which are obtained from (4.9) by simple matrix inversion. In order to set up the matrix on the left-hand side of (4.9), we have to calculate the structure function F_L, which, in (4.7) is given in its series representation. This representation is useless for the actual computation of F_L, since the sum is only conditionally, and therefore very slowly, convergent. The problem can be solved by a suitable resummation of the series (4.7) and the resulting convergence accelerated formuli are presented in appendix B. We also present a recurrence scheme which allows for a fast evaluation of F_L by upward and downward recurrence in L in case many partial waves are needed.

The theory presented above has the advantage that the calculation of the S-matrix is essentially reduced to the algebraic problem of inverting a matrix thereby circumventing the usual way of calculating the S-matrix by solving numerically the differential equations for the scattering wavefunctions.

5. Numerical results

The most prominent feature of our scattering model is the fact that classically it displays a transition from "regular" to "irregular" scattering as a function of the control parameter Θ_{max}, the maximal deflection angle. The critical value $\Theta_{max}^{(c)}$ which characterizes the transition between the two scattering domains is given in (3.1c). In this section we will show that a similar transition happens also in the quantum version of our model, and that the transition point is very close to the classical value. We will show that the S-matrix behaves quite differently in the two regimes, and that in the classically chaotic domain, the predictions (a)–(d) of the semi-classical theory presented in section 3 above are fulfilled to a high degree of accuracy. We start by studying the fluctuation of the S-matrix in the classically chaotic domain. Taking $d/D = 0.99$ and $v_0/E = 20$ we get $\Theta_{max} = 80$ which brings us well above the transition value $\Theta_{max}^{(c)} = 4.6$. The semi-classical regime corresponds to situations where the dimension of the Bragg manifold N_B is large. We chose $\hbar^2 = 10^{-5}$ in our units so that $N_B = 100$. To get sufficient statistics we vary the energy in a "small" interval $1.0 < E < 1.012$, which, however, is a factor 60 larger than the width $\hbar\gamma = 2 \times 10^{-4}$ of the energy auto correlation function (see figs. 7, 8). Unless specified otherwise, we used the above set of parameters for all the results shown in figs. 2–6.

The nearest neighbour distribution of the eigenvalues of the S-matrix on the unit circle is very well reproduced by a Wigner function (fig. 2(b)), as predicted by (a) in section 3.

The distributions of $|S_{ii}|^2$ and $|S_{i,i+1}|^2$ are shown in fig. 3(a, b)) and they agree very well with the random matrix predictions (compare (b) of section 3).

We repeated the quantum calculation for the same conditions, changing only the value of v_0 to 0.2. This corresponds to $\Theta_{max} = 0.8$ which brings us well within the classically regular domain. Here, the nearest neighbour distribution of the eigenvalues of the S-matrix (fig. 2(a)) as well as the statistics of the S-matrix elements (fig. 3(c, d)) depart considerably from the random matrix predictions.

To study the quantum transition in a quantitative way, we perform the following numerical experiment. We calculated the three distributions mentioned above for a large range of Θ_{max} values, this time using a larger value of $\hbar^2$ so that $N_B = 30$. At each Θ_{max} the statistics was improved by averaging over 150

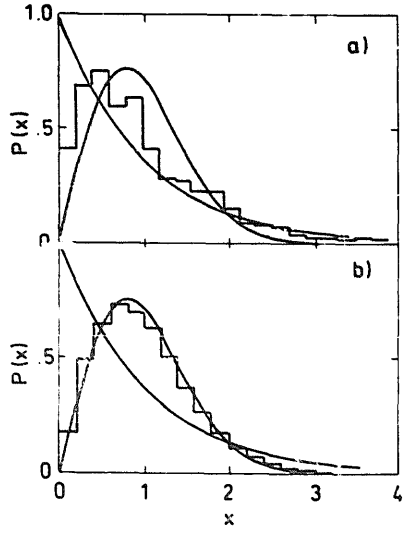

Fig. 2. Nearest neighbour spacings distribution for classically regular (a) and irregular (b) scattering. The variable x measures the spacings in units of the mean spacing $2\pi/N_B$. The smooth curves are the Poisson and Wigner distributions.

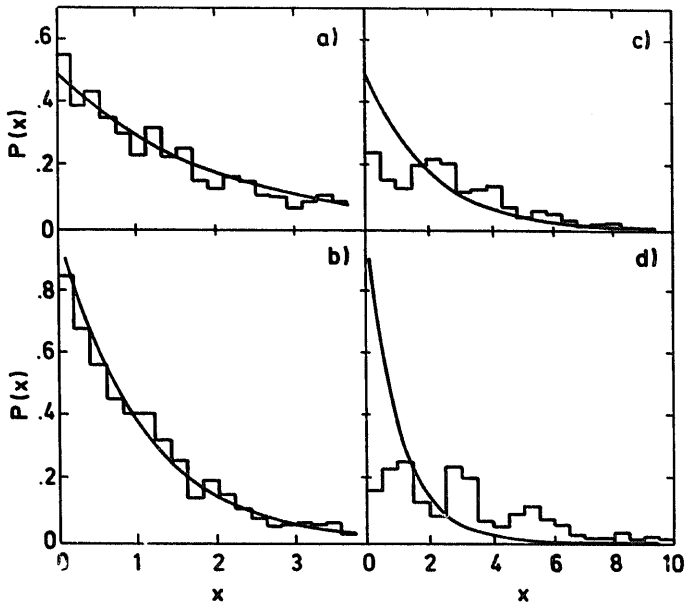

Fig. 3. Distributions of diagonal and off-diagonal S-matrix elements. (a,b) Classically irregular scattering, (c,d) classically regular scattering. x measures $|S|^2$ in units of $1/N_B$.

S-matrices for the incident angles 67, 70 and 73 degrees and 50 values of the energy ($\Delta E = 2 \times 10^{-3}$) for each angle. The degree of agreement between the random ensemble prediction and the numerical distributions was tested by calculating

$$\chi^2(\Theta_{\max}) = \frac{1}{H} \sum_{i=1}^{H} \left(\frac{N_i - T_i}{E_i} \right)^2, \tag{5.1}$$

where N_i and T_i are the numerical and theoretical values for the ith bin of the distribution, $H(=20)$ is the number of bins considered and E_i is the error estimate of N_i which is due to the counting statistics. Fig. 4(a–c) show the values of $\chi^2(\Theta_{\max})$ for the nearest neighbour, the $|S_{ii}|^2$ and $|S_{i,i+1}|^2$ distributions as a log–log plot, respectively. The most important feature is the sharp transition which occurs in the vicinity of $\Theta_{\max}^{(c)} = 4.6$ (shown as an arrow in the figure). As soon as $\Theta_{\max}$ exceeds $\Theta_{\max}^{(c)}$, the quality of the fit reaches in all three cases the asymptotic value. This value ranges between 1 and 4 for the matrix elements distributions, and between 3 and 9 for the nearest neighbour distribution. The deviations of χ^2 from the expected value 1 may be due to a too conservative estimate of the errors E_i or to a systematic deviation between the numerical experiments and the theory. We have some grounds to believe that the latter is responsible in part for the deviations, and better χ^2-values were systematically obtained for larger N_B-values (smaller $\hbar$). Unfortunately, limitations of computer resources do not allow us to repeat the calculations for larger values of N_B. The sharp increase of $\chi^2(\Theta_{\max})$ at $\Theta_{\max} < \Theta_{\max}^{(c)}$ is remarkable, and should be related to the abrupt change of the corresponding classical dynamics. A more detailed study of the classical transition and its quantum implications is now in progress.

Our proposal that the S-matrix in the chaotic regime represents a typical member of the Dyson ensemble followed from the semi-classical result (3.14). We calculated numerically diagonal and off-diagonal correlations $F_{nm}(\eta)$ and we illustrate the results in fig. 5. They meet the expectation to a high degree of accuracy.

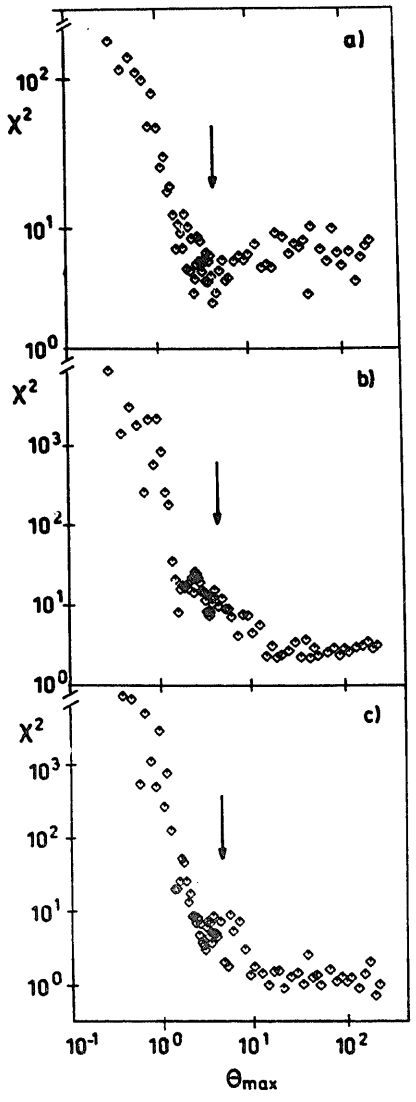

Fig. 4. Quality of agreement between the quantum distributions and the random ensemble predictions as a function of the classical maximal deflection angle Θ_{max}. The arrow marks the transition to the onset of classical chaos. (a) Nearest neighbour spacing distribution, (b) $|S_{ii}|^2$ distribution and (c) $|S_{i,i+1}|^2$ distribution.

An important test of the statistical properties of the ensemble are the values of the correlation function $\tilde{F}_{nm}(\eta) = N_B\langle S_{nm}S_{n,m+\eta}\rangle_n$ which is defined similarly to (3.11) with one important difference: it measures the correlations between S and itself, and *not* of S with $S^\dagger$. The functions $\tilde{F}_{nm}(\eta)$ should vanish for all η, once the basis N_B and the averaging interval Δ are sufficiently large. The function $\tilde{F}_{nm}(\eta)$ is shown in fig. 5 as a dashed line for the same transition as the function $F_{nm}(\eta)$. Its mean value represents the mean square of the fluctuations. We checked that it depends on the basis size and the averaging sample as expected.

We now turn to the study of the energy fluctuations and their correlations. We first compare the transition probabilities $|S^{(-)}_{71,81}(E)|^2$ calculated for $\Theta_{max} = 0.8$ and $\Theta_{max} = 80$ with otherwise identical set of parameters and range (fig. 6). The difference between the smooth behaviour of $|S_{ij}|^2$ in the regular regime (see fig. 6(a)) and the fluctuations in the irregular regime (fig. 6(b)) is apparent, and typical. The abrupt

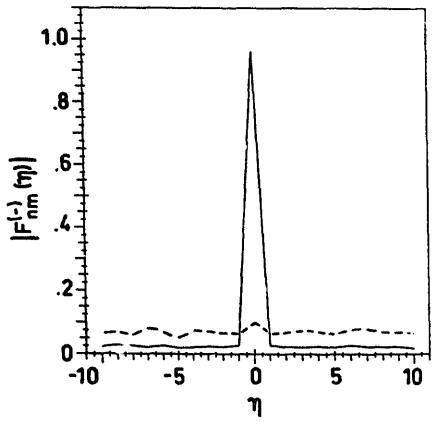

Fig. 5. The correlation functions $|F^{(-)}_{nm}(\eta)|$ (full line) and $|\tilde{F}^{(-)}_{nm}(\eta)|$ (dashed line) for $n = 56$ and $m = 63$.

change in the regular transition amplitude at $E = 1.0026$ is due to a threshold which corresponds to the emergence of a new accessible Bragg direction at this energy. The same threshold must also affect the transition probability for $\Theta_{max} = 80$, but it is hard to distinguish it on the background of the rapid fluctuations. Another discontinuity in fig. 6(a) can be observed at energy $E = 1.006$. Here, l_{max} increases by 1. This discontinuity is an artifact of our model ($\sigma_l = 0$ for $l > l_{max}$) and does not have any physical significance.

The fluctuating transition amplitudes for the classically chaotic case are used as a basis for the auto-correlation analyses (point (d) of section 3). We chose at random a sample of pairs of indices (n_i, m_i),

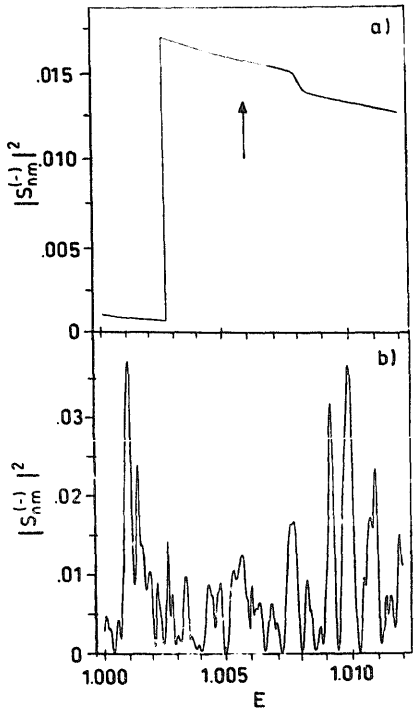

Fig. 6. Dependence of the transition probabilities $|S^{(-)}_{n,m}|^2$ for $n = 71$, $m = 81$ on the energy in the classically regular (a) and irregular (b) cases. The arrow in (a) marks the energy at which l_{max} grows by one unit (see text).

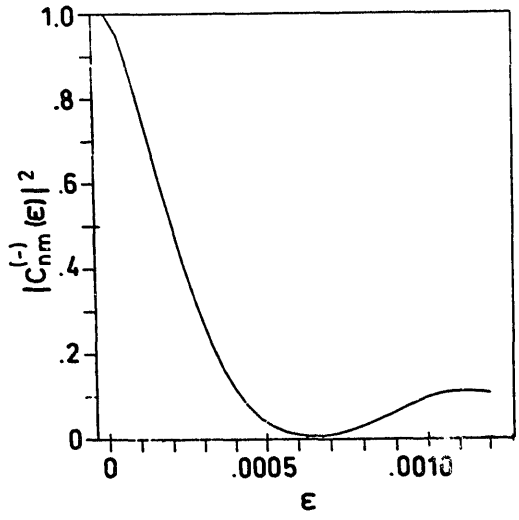

Fig. 7. The energy auto-correlation function which corresponds to the amplitudes shown in fig. 6(b).

$i = 1, \ldots, 10$ and calculated the absolute square of the auto-correlation functions (3.17). A typical example is shown in fig. 7. The half-width at half-maximum was deduced for each of the index pairs (n_i, m_i), and their mean and standard deviation were calculated. A summary of our numerical results is shown in fig. 8. Here, five different sets of data are shown, and they differ only in the value of $\hbar$. (The corresponding N_B vary between 100 and 10.) From this figure we see that: (i) For any given value of $\hbar$, the widths are constant to within 20%. In view of the uncertainty in the method by which we extract the width (finite sample size, finite energy resolution, etc.), this range of variability of the width extracted from different pairs (n_i, m_i) is acceptable. (ii) The mean value of the width is proportional to $\hbar$ as predicted by (3.17). (iii) The numerical widths are compared to the classical prediction in terms of the parameter γ (dashed line). It should be noted that for a detailed numerical comparison of the quantal and classical results, the parameter γ extracted in CT is insufficient. It measures the distribution of the number of scatterings but not of the dwell times. A rough estimate of the dwell time in terms of the number of scatterings is obtained

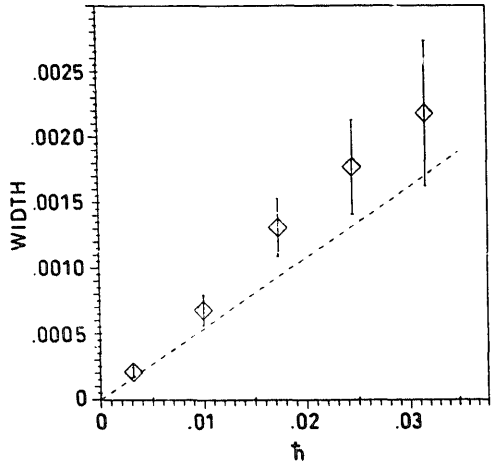

Fig. 8. Dependence of the half-width at half-maximum of the energy auto-correlation function as a function of $\hbar$. The dashed line gives the semi-classical estimate.

by taking the mean dwell time per scattering $\langle 2\hbar\,\partial\sigma_l/\partial E\rangle$ as the factor which scales the two distributions. But, since different dwell times can be obtained for the same number of scatterings we had to convolute the two distributions to get an accurate result. We iterated the classical scattering map numerically and deduced the proper parameter γ which is displayed in the figure. It differs by a factor of approximately 2 from the simple scaling estimate.

The quantum widths seem to be systematically higher than the classical data. If we remember, however, that the numerical estimate of the classical γ is also good only to within 10%, we would get good overlap between the numerical and the theoretical predictions.

We can summarize our numerical investigation by noting that the exact quantum results reproduce satisfactorily the semi-classical predictions. They also provide intriguing evidence for an abrupt transition in the quantum statistics which coincides with the abrupt classical transition from the regular to the chaotic domain.

6. Discussion and summary

In the present work we brought some semi-classical arguments and numerical evidence to support our conjecture that "quantum chaos" in the domain of scattering is manifested in the fluctuations of cross sections and their statistics. The random character of the fluctuations can be observed in various independent ways. The dependence of the scattering matrix elements $S_{n,m}(E)$ on the indices n or m (for a constant E), or its dependence on E (for fixed n, m) show fluctuations of similar nature and origin. In the problem studied here the indices n, m are discrete and it was shown that the fluctuations follow the predictions of the statistics of Dyson's orthogonal ensemble. The fact that the S-matrix is computed within a deterministic theory introduces correlations between S-matrices which correspond to different energies. Statistical independence is achieved only if the energy difference exceeds the correlation range $\hbar\gamma$.

The fluctuations of the cross sections in energy and their typical auto-correlation and statistics are reminiscent of Ericson fluctuations which are encountered in nuclear reactions. The origin of these fluctuations is intimately connected with the poles of the S-matrix in the complex E plane. Once the mean spacing between the poles is smaller than the mean width, one observes Ericson fluctuations in the cross section. In the present paper we have shown that the Ericson condition is always met in the limit $\hbar \to 0$. A similar argument applies also for the origin of the fluctuations in the scattering phase for the problem of scattering on a surface of negative curvature [16]. One can easily estimate the ratio between the mean spacing of the resonances and their widths as a function of the wave number w, which is given by $2\pi/|\ln(w/\pi)|$. For small w the spacing exceeds the width and one can attribute the structure in the phase to specific resonances. For w values larger than $w_c = \pi e^{2\pi} \approx 1682$ this is not the case. The Ericson condition is fulfilled and the phase shows much more structure and oscillations than could be assigned to specific resonances. This is the regime which Gutzwiller denotes as chaotic.

For quite some time [27] already, the mathematical literature is concerned with the problem of finding general properties of the distribution of the poles of the S-matrix for a given scattering problem. There exist, e.g., theorems which specify the regions in the complex plane where most of the poles are located for scattering in 3 dimensions from two convex and non-overlapping ideal reflectors [28, 29]. The fact that the distribution of S-matrix poles has to do with the set of "trapped" classical trajectories is appreciated and discussed in the literature. To the best of our understanding there are no exact results relating the properties of the pole distribution to the dynamics of the trapped trajectories when the latter are in the chaotic domain.

Acknowledgements

We would like to thank Profs. P. Mello, P. Brumer, M. Berry and H.A. Weidenmüller for good advice and interesting discussions during the time this work was under way. It is a pleasure to acknowledge G. Troll for his important contributions to the development of the classical theory. One of us (US) would like to thank Prof. H. Walther for the hospitality during his visit at the MPQ. This research was supported in part by a grant from the German–Israeli foundation for scientific research and development (GIF).

Appendix A

Lattice Green's function and structure function

In (4.6) the Lattice Green's function is defined as

$$g_k^{(+)}(r; r') = \sum_{n=-\infty}^{\infty} G_k^{(+)}(r; r' + r_n)\, e^{in\alpha D}, \quad 0 \le |r'| \le |r| \le D/2, \tag{A.1}$$

where $r_n = nDe_y$, and $G_k^{(+)}(r; r')$ is given explicitly by (see ref. [18], p. 811, (7.2.18))

$$G_k^{(+)}(r; r') = i\pi H_0^{(+)}(k|r - r'|). \tag{A.2}$$

We evaluate (A.1) by repeated application of the formula [25]

$$e^{il\Phi_{a+b}} H_l^{(+)}(|a + b|) = \sum_{l'=-\infty}^{\infty} H_{l-l'}^{(+)}(|b|)\, J_{l'}(|a|)\, e^{i[(l-l')\Phi_b + l'\Phi_a]}, \quad |b| > |a|. \tag{A.3}$$

For the condition specified in (A.1) and $n \neq 0$ we have $|r' + r_n| > r$ and the first application of (A.3) yields

$$G_k^{(+)}(r; r' + r_n) = i\pi \sum_{l=-\infty}^{\infty} e^{il\Phi_{r'+r_n}} H_l^{(+)}(k|r' + r_n|)\, J_l(kr)\, e^{-il\Phi_r}. \tag{A.4}$$

Now, $|r_n| > |r'|$ and a second application of (A.3) yields

$$G_k^{(+)}(r; r' + r_n) = i\pi \sum_{ll'=-\infty}^{\infty} H_{l-l'}^{(+)}(Dk|n|)\, J_l(kr)\, J_{l'}(kr')\, e^{i(\pi/2)(l-l')\operatorname{sign}(n)} e^{i(l'\Phi_{r'} - l\Phi_r)}. \tag{A.5}$$

With (A.5) and including the contribution from $n = 0$, the total Lattice Green's function finally becomes:

$$g_k^{(+)}(r; r') = i\pi \sum_{ll'=-\infty}^{\infty} \left\{\delta_{ll'} H_l^{(+)}(kr) + F_{l-l'}(Dk, D\alpha)\, J_l(kr)\right\} J_{l'}(kr')\, e^{i[l\Phi_r - l'\Phi_{r'}]}, \tag{A.6}$$

where we introduced the structure function

$$F_L(x, y) = 2 \sum_{n=1}^{\infty} H_L^{(+)}(nx) \cos\left[ny - L\frac{\pi}{2}\right], \quad |y| \le x, \quad x > 0. \tag{A.7}$$

The following symmetries of the structure function are immediately apparent:

$$F_{-L}(x, y) = F_L(x, y) = (-1)^L F_L(x, -y),$$
$$F_L(x, y + 2m\pi) = F_L(x, y), \quad m \in \mathbb{Z}. \tag{A.8}$$

Appendix B

Evaluation of the structure function

For the real part of the structure function explicit expressions are available, which we will derive as follows:

$$\begin{aligned}\mathrm{Re}\{F_L(x, y)\} &= 2\sum_{n=1}^{\infty} J_L(nx)\cos\left(ny - L\frac{\pi}{2}\right) \\ &= \mathrm{Re}\left\{\int_{-\pi}^{\pi} e^{-iL\theta} e^{iL\pi/2}\,\delta_{2\pi}(x\sin(\theta) - y)\,d\theta\right\} - \delta_{L0} \\ &= 2\int_{-\pi/2}^{\pi/2} \cos\left[L\left(\frac{\pi}{2} - \theta\right)\right]\delta_{2\pi}(x\sin(\theta) - y)\,d\theta - \delta_{L0}.\end{aligned} \tag{B.1}$$

We used the integral representation of the Bessel functions (ref. [30], 8.4111) and summed over n to obtain the 2π-periodic δ-function. In the following we will assume $y > 0$ which can always be achieved with the help of (A.8). We define

$$\eta = y \bmod (2\pi), \quad \eta_m = \frac{2m\pi + \eta}{x}, \quad \bar{\eta}_m = \frac{2m\pi - \eta}{x} \tag{B.2}$$

and integers ν and μ such that

$$\eta_\nu < 1 < \eta_{\nu+1}, \quad \bar{\eta}_\mu < 1 < \bar{\eta}_{\mu+1}. \tag{B.3}$$

Then

$$\begin{aligned}\mathrm{Re}\{F_L(x, y)\} &= 2\left\{\sum_{m=0}^{\nu} \cos\left[L\left(\frac{\pi}{2} - \theta_m\right)\right]\frac{1}{x\cos\theta_m} + \sum_{m=1}^{\mu} \cos\left[L\left(\frac{\pi}{2} - \bar{\theta}_m\right)\right]\frac{1}{x\cos\bar{\theta}_m}\right\} - \delta_{L0} \\ &= \frac{2}{x}\left\{\sum_{m=0}^{\nu} \frac{T_L(\eta_m)}{\sqrt{1-\eta_m^2}} + \sum_{m=1}^{\mu} \frac{T_L(\bar{\eta}_m)}{\sqrt{1-\bar{\eta}_m^2}}\right\} - \delta_{L0},\end{aligned} \tag{B.4}$$

where

$$\theta_m = \arcsin(\eta_m), \quad 0 \le m \le \nu,$$
$$\bar{\theta}_m = \arcsin(\bar{\eta}_m), \quad 1 \le m \le \mu, \tag{B.5}$$

and

$$T_L(x) = \cos[L \arccos(x)], \quad T_0 = 1, \quad T_1 = x,$$
$$T_{L+1} = 2xT_L(x) - T_{L-1}(x) \tag{B.6}$$

are Tshebyscheff's polynomials of the first kind, which can safely be calculated in upward recurrence.

The imaginary part of the structure function,

$$\mathrm{Im}\{F_L(x, y)\} = 2\sum_{n=1}^{\infty} Y_L(nx)\cos\left(ny - L\frac{\pi}{2}\right), \tag{B.7}$$

is calculated with the help of a recursive scheme. We define the moments

$$C_L^M(x, y) = \sum_{n=1}^{\infty} \frac{1}{n^M} Y_L(nx)\cos(ny),$$
$$S_L^M(x, y) = \sum_{n=1}^{\infty} \frac{1}{n^M} Y_L(nx)\sin(ny), \quad L, M \geq 0, \tag{B.8}$$

which satisfy the recurrence relations

$$C_{L+1}^M(x, y) = \frac{2L}{x} C_L^{M+1}(x, y) - C_{L-1}^M(x, y),$$
$$S_{L+1}^M(x, y) = \frac{2L}{x} S_L^{M+1}(x, y) - S_{L-1}^M(x, y). \tag{B.9}$$

The "C" and the "S" moments do not couple. We have

$$\mathrm{Im}\{F_L(x, y)\} = 2\left\{C_L^0(x, y)\cos\left(L\frac{\pi}{2}\right) + S_L^0(x, y)\sin\left(L\frac{\pi}{2}\right)\right\}. \tag{B.10}$$

In order to close the recurrence in M-direction, we choose $M_0 \geq 0$ and calculate $C_L^{M_0+1}(x, y)$ and $S_L^{M_0+1}(x, y)$ by direct summation of (B.6), which already for $M_0 = 5$ converges very quickly. In order to start the recurrence in L-direction, we need $C_L^M(x, y)$, $S_L^M(x, y)$, $L = 0, 1$; $M = 0, \ldots, M_0$. For C_0^0 we use the convergence accelerated formula (ref. [30], 8.5223):

$$C_0^0(x, y) = \sum_{n=1}^{\infty} Y_0(nx)\cos(ny)$$
$$= -\frac{1}{\pi}\left\{C + \ln\left(\frac{x}{4\pi}\right)\right\} + \frac{1}{2\pi}\left\{\sum_{m=1}^{\nu}\frac{1}{m} + \sum_{m=1}^{\mu}\frac{1}{m}\right\}$$
$$- \sum_{m=\nu+1}^{N}\left\{\frac{1}{x\sqrt{\eta_m^2 - 1}} - \frac{1}{2\pi m}\right\} - \sum_{m=\mu+1}^{N}\left\{\frac{1}{x\sqrt{\eta_m^2 - 1}} - \frac{1}{2\pi m}\right\} - \gamma_0^0(x, \eta; N), \tag{B.11}$$

where $C = 0.5772\ldots$ is Euler's constant and $\gamma_0^0(x, \eta; N) \sim (x^2 + 2\eta^2)/16\pi^3 N^2$ to leading order in N.

Define

$$\xi = x \bmod 2\pi, \qquad \eta_0 = \begin{cases} 0 & \text{if } \eta < \xi,\ \eta + \xi < 2\pi, \\ \pi & \text{if } \eta < \xi,\ \eta + \xi > 2\pi, \\ \pi & \text{if } \eta > \xi,\ \eta + \xi < 2\pi, \\ 2\pi & \text{if } \eta > \xi,\ \eta + \xi > 2\pi \end{cases} \tag{B.12}$$

and

$$\eta_m^0 = \frac{2m\pi + \eta_0}{x}, \qquad \bar{\eta}_m^0 = \frac{2m\pi - \eta_0}{x}. \tag{B.13}$$

Then

$$\begin{aligned} S_0^1(x, y) &= \sum_{n=1}^{\infty} \frac{1}{n} Y_0(nx) \sin(ny) = \int_{\eta_0}^{\eta} C_0^0(x, \eta')\, \mathrm{d}\eta' \\ &= \frac{\eta - \eta_0}{2\pi} \left\{ -2C - 2\ln\left(\frac{x}{4\pi}\right) + \sum_{m=1}^{\nu} \frac{1}{m} + \sum_{m=1}^{\mu} \frac{1}{m} \right\} \\ &\quad - \sum_{m=\nu+1}^{N} \left\{ \ln\left[\frac{\eta_m + \sqrt{\eta_m^2 - 1}}{\eta_m^0 + \sqrt{(\eta_m^0)^2 - 1}} \right] - \frac{\eta - \eta_0}{2\pi m} \right\} \\ &\quad + \sum_{m=\mu+1}^{N} \left\{ \ln\left[\frac{\bar{\eta}_m + \sqrt{\bar{\eta}_m^2 - 1}}{\bar{\eta}_m^0 + \sqrt{(\bar{\eta}_m^0)^2 - 1}} \right] + \frac{\eta - \eta_0}{2\pi m} \right\} - \sigma_0^1(x, \eta; N) \end{aligned} \tag{B.14}$$

and $\sigma_0^1(x, \eta; N) = \int_{\eta_0}^{\eta} \gamma_0^0(x, \eta'; N)\, \mathrm{d}\eta' \sim (1/16\pi^3 N^2)\{x^2(\eta - \eta_0) + \frac{2}{3}(\eta^3 - \eta_0^3)\}$. Differentiating (B.14), we get an expression for the moment S_1^0:

$$\begin{aligned} S_1^0(x, y) &= \sum_{n=1}^{\infty} Y_1(nx) \sin(ny) = -\sum_{n=1}^{\infty} Y_0'(nx) \sin(n\eta) = -\frac{\partial}{\partial x} S_0^1(x, \eta) \\ &= \frac{\eta - \eta_0}{\pi x} - \frac{1}{x} \sum_{m=\nu+1}^{N} \left\{ \frac{\eta_m}{\sqrt{\eta_m^2 - 1}} - \frac{\eta_m^0}{\sqrt{(\eta_m^0)^2 - 1}} \right\} \\ &\quad + \frac{1}{x} \sum_{m=\mu+1}^{N} \left\{ \frac{\bar{\eta}_m}{\sqrt{\bar{\eta}_m^2 - 1}} - \frac{\bar{\eta}_m^0}{\sqrt{(\bar{\eta}_m^0)^2 - 1}} \right\} + \sigma_1^0(x, \eta; N) \end{aligned} \tag{B.15}$$

and $\sigma_1^0(x, \eta; N) = \partial \sigma_0^1(x, \eta; N)/\partial x \sim x(\eta - \eta_0)/8\pi^3 N^2$. We use the integral representation (ref. [30],

8.4154) to derive

$$S_0^0(x, y) = \sum_{n=1}^{\infty} Y_0(nx)\sin(ny)$$

$$= \frac{1}{x}\sum_{m=0}^{\nu}\frac{1}{\sqrt{1-\eta_m^2}} - \frac{1}{x}\sum_{m=1}^{\mu}\frac{1}{\sqrt{1-\bar{\eta}_m^2}} - \frac{1}{\pi}\int_0^{A(\epsilon)}\frac{\sin(\eta)}{\cosh[x\sinh(t)]-\cos(\eta)}\,dt. \tag{B.16}$$

If the integral is required to an absolute accuracy ϵ, then the upper integration limit should be $A(\epsilon) > \operatorname{arcsinh}[(1/x)\ln(2/\epsilon)]$. The integral in (B.16) can be evaluated by any standard procedure.

The same integral representation (ref. [30], 8.4154) is used together with

$$\sum_{n=1}^{\infty}\frac{\sin(nx)}{n} = \frac{\pi-\xi}{2} \tag{B.17}$$

and

$$\sum_{n=1}^{\infty}\frac{\lambda^n}{n} = -\ln(1-\lambda) \tag{B.18}$$

to obtain

$$C_0^1(x, y) = \sum_{n=1}^{\infty}\frac{1}{n}Y_0(nx)\cos(ny)$$

$$= \frac{\pi}{2}(\mu+\nu+1) - \frac{x}{\pi} - \left\{\sum_{m=0}^{\nu}\theta_m + \sum_{m=1}^{\mu}\bar{\theta}_m\right\}$$

$$+ \frac{1}{\pi}\int_0^{A(\epsilon)}\ln\left[1-2\cos(\eta)\,e^{-x\sinh(t)}+e^{-2x\sinh(t)}\right]dt. \tag{B.19}$$

The C_1^0 moments are obtained by differentiating (B.19):

$$C_1^0(x, y) = \sum_{n=1}^{\infty}Y_1(nx)\cos(ny) = -\frac{\partial}{\partial x}C_0^1(x, y)$$

$$= \frac{1}{\pi} - \frac{1}{x}\sum_{m=0}^{\nu}\left\{\frac{\eta_m}{\sqrt{1-\eta_m^2}}\right\} - \frac{1}{x}\sum_{m=1}^{\mu}\left\{\frac{\bar{\eta}}{\sqrt{1-\bar{\eta}_m^2}}\right\}$$

$$- \frac{1}{\pi}\int_0^{A(\epsilon)}\frac{\sinh(t)[\cos(\eta)-e^{-x\sinh(t)}]}{\cosh[x\sinh(t)]-\cos(\eta)}\,dt. \tag{B.20}$$

Integrating the C_1^0 moment on η, we get

$$S_1^1(x,y)=\sum_{n=1}^{\infty}\frac{1}{n}Y_1(nx)\sin(n\eta)=\int_{\eta_0}^{\eta}C_1^0(x,\eta')\,d\eta'$$

$$=\frac{\eta-\eta_0}{\pi}+\sum_{m=0}^{\nu}\left\{\sqrt{1-\eta_m^2}-\sqrt{1-(\eta_m^0)^2}\right\}-\sum_{m=1}^{\mu}\left\{\sqrt{1-\bar{\eta}_m^2}-\sqrt{1-(\bar{\eta}_m^0)^2}\right\}$$

$$-\frac{1}{\pi}\int_0^{A(\epsilon)}\sinh(t)\left\{2\arctan\left[\frac{\sinh(x\sinh(t))\tan(\eta/2)}{\cosh(x\sinh(t))-1}\right]-\eta+\Phi(\eta)\right\},\tag{B.21}$$

where

$$\Phi(\eta)=\begin{cases}0 & \text{if } \eta<\pi,\\ 2\pi & \text{if } \eta>\pi.\end{cases}\tag{B.22}$$

Using the integral representation (ref. [30], 8.4152) together with

$$\sum_{n=1}^{\infty}\frac{\cos(nx)}{n^2}=\frac{\pi^2}{6}-\frac{\pi}{2}\xi+\frac{1}{4}\xi^2\tag{B.23}$$

we derive

$$C_1^1(x,y)=\sum_{n=1}^{\infty}\frac{1}{n}Y_1(nx)\cos(ny)=-\frac{\partial}{\partial x}\sum_{n=1}^{\infty}\frac{1}{n^2}Y_0(nx)\cos(n\eta)$$

$$=f_{\nu+1;\nu}(x,\eta)+\bar{f}_{\mu+1;\mu}(x,\eta)+\sum_{m=\nu+1}^{N}\{f_{m+1;m}(x,\eta)-f_{m;m}(x,\eta)\}$$

$$+\sum_{m=\mu+1}^{N}\{\bar{f}_{m+1;m}(x,\eta)-\bar{f}_{m;m}(x,\ )\}+\gamma_1^1(N),\tag{B.24}$$

where

$$f_{mp}(x,\eta)=\frac{x}{4\pi}\left[\eta_m\sqrt{\eta_m^2-1}+\ln\left(\eta_m+\sqrt{\eta_m^2-1}\right)\right]-\frac{1}{2\pi}[\eta+(2p+1)\pi]\sqrt{\eta_m^2-1}$$

$$-\frac{\eta_m}{2x\pi\sqrt{\eta_m^2-1}}\left\{\frac{1}{2}(x\eta_m)^2-x\eta_m[\eta+(2p+1)\pi]+\frac{1}{2}[\eta+(2p+1)\pi]^2-\frac{\pi^2}{6}\right\},\tag{B.25}$$

$$\bar{f}_{mp}(x,\eta)=f_{mp}(x,-\eta)$$

and $\gamma_1^1(N)\sim o(N^{-4})$.

For $M\geq 2$ the series (B.8) are absolutely convergent and the remaining moments $C_L^M(x,y)$, $S_L^M(x,y)$, $L=0,1$; $M=2,\ldots,M_0$ are calculated by direct summation of (B.8).

The method outlined above enables one to calculate the structure function to any desired accuracy. The error estimates are useful to determine the number of terms one has to sum up to achieve the prescribed accuracy.

References

[1] G. Troll and U. Smilansky, Physica D 35 (1989) 34.
[2] A similar model was introduced recently in a different context by W.J. Firth, Phys. Rev. Lett. 61 (1988) 329.
[3] R. Blümel and U. Smilansky, Phys. Rev. Lett. 60 (1988) 477–480.
[4] T. Ericson, Phys. Rev. Lett. 5 (1960) 430–431.
[5] T. Ericson and T. Mayer-Kuckuk, Ann. Rev. Nucl. Sci. 16 (1966) 183–206.
[6] T. Ericson, Ann. Phys. 23 (1963) 390–414.
[7] D.M. Brink and R.O. Stephen, Phys. Lett. 5 (1963) 77–79.
[8] F.J. Dyson, J. Math. Phys. 3 (1962) 140.
[9] C.E. Porter, Statistical Theory of Spectral Fluctuations (Academic Press, New York, 1965).
[10] C.E. Porter and R.G. Thomas, Phys. Rev. 104 (1956) 483.
[11] M. Kawai, A.K. Kerman and K.W. McVoy, Ann. Phys. 75 (1973) 156.
[12] D. Agassi, H.A. Weidenmüller and G. Mantzouranis, Phys. Rep. C 22 (1975) 145.
[13] T.A. Brody, J. Flores, J.B. French, P.A. Mello, A. Pandey and S.S.M. Wong, Rev. Mod. Phys. 53 (1981) 385.
[14] O. Bohigas, M.J. Giannoni and C. Schmit, Phys. Rev. Lett. 52 (1984) 1–4.
[15] M.V. Berry, Proc. Roy. Soc. London A 400 (1985) 229.
[16] M.C. Gutzwiller, Physica D 7 (1983) 341–355.
[17] P. Brumer and M. Shapiro, Adv. Chem. Phys. 70 (1988) 365.
[18] P.M. Morse and H. Feshbach, Methods of Theoretical Physics, part I + II (McGraw-Hill, New York, Toronto, London 1953).
[19] L.D. Landau and E.M. Lifshitz, Quantum Mechanics, 2nd ed. (Pergamon, New York, 1965).
[20] G. Troll and U. Smilansky, in preparation.
[21] W.H. Miller, Adv. Chem. Phys. 30 (1975) 77–136.
[22] V.P. Maslov, USSR Comp. Math. Phys. 3 (1962) 744.
[23] P. Pereyra and P.A. Mello, J. Phys. A 16 (1983) 237–254.
[24] J. Koringa, Physica 13 (1947) 392. W. Kohn and N. Rostoker, Phys. Rev. 94 (1954) 1111–1124.
[25] M.V. Berry, Ann. Phys. NY 131 (1981) 163–216.
[26] A.M. Ozorio de Almeida, Acta Cryst. A 31 (1975) 435–442, 442–445.
[27] P.D. Lax and R.S. Phillips, Scattering Theory (Academic Press, New York, 1967).
[28] M. Ikawa, J. Math. Kyoto Univ. 23 (1983) 127, 795.
[29] C. Gerard and J. Sjöstrand, Commun. Math. Phys. 108 (1987) 391.
[30] I.S. Gradshteyn and I.M. Ryzhik, Table of Integrals, Series and Products (Academic Press, New York, 1980).